OPTICAL FIBER TECHNOLOGY **4,** 371–383 (1998)
ARTICLE NO. OF980265

Impulse Response of Cross-Phase Modulation Filters in Multi-span Transmission Systems with Dispersion Compensation

Alberto Bononi, Cristian Francia, and Giovanni Bellotti

Dipartimento di Ingegneria dell'Informazione, Università di Parma, Parma, Italy

Received December 12, 1997

As shown by Chiang *et al*. (1996), cross-phase modulation on each channel of a wavelength-division-multiplexed transmission system can be viewed as a phase modulation, where the modulating signal is the sum of the input intensities of all the other copropagating channels, each filtered by a low-pass filter, whose bandwidth decreases with the walk-off parameter. We give an explicit expression of the impulse response of such filter in the general case of dispersion mapped transmission systems. We show by simulation that this filter, in intensity-modulated transmission systems, gives an optimal prediction of the signal phase even when the underlying assumption of negligible envelope distortion upon which its derivation is based is strongly violated. As an application, we show an analytical evaluation of the spectral broadening induced by XPM in multi-span compensated systems. © 1998 Academic Press

I. INTRODUCTION

In a fundamental paper, Chiang *et al*. [1] have shown that cross-phase modulation (XPM) in wavelength-division-multiplexed (WDM) optical transmission systems can be modeled as a phase modulator with inputs from the intensity of copropagating waves. Such inputs are low-pass filtered by the relative channel walk-off induced by chromatic dispersion: the larger the walk-off, the narrower the filter bandwidth. This model nicely explains the weak dependence of XPM on the number of WDM channels, which has already been observed experimentally and by simulation in [2]. Chiang *et al*. [1] have extended such a model to cascades of ideally amplified fiber links with dispersion compensation.

This paper provides a time-domain derivation of the theoretical model proposed in [1], leading to an explicit expression of the filter impulse response, both for a single fiber span and for a cascade of amplified links with dispersion compensation.

1068-5200/98 $25.00
Copyright © 1998 by Academic Press
All rights of reproduction in any form reserved.

We find that the expression of the filter phase in [1] is incorrect because of an inconsistency in the use of Fourier transforms.

Having the correct phase expression, we show that such a filter is noncausal when the interfering channel travels faster than the observed channel. In such a case, the phase of the interfering channel at the detector contains information about the future information bits of the observed channel.

We give a graphical interpretation of the filter impulse response in the case of link-by-link dispersion compensation in a cascade of amplified links, so that the periodic forward and backward relative walk-off becomes apparent.

For the case of intensity-modulation direct-detection (IM/DD) systems, we provide simulation evidence that the model surprisingly holds even though the assumption of negligible envelope distortion upon which its derivation is based is strongly violated. In other words, we find that the modulation induced on the optical field phase by XPM is nearly independent of the distortion induced on the intensity of the optical field by group velocity dispersion (GVD). This is due to the above-mentioned low-pass filtering effect of chromatic dispersion-induced channel walk-off on XPM.

An an application of the filter impulse response, we give an analytical evaluation of the spectral broadening induced by XPM in multi-span compensated systems.

The paper is organized as follows. Section II provides the derivation of the filter impulse response for a single link, while Section III extends it to the general case of dispersion-compensated cascades of amplified fiber links. Section IV presents simulation results providing evidence that the model holds even in the presence of strong intensity distortion due to group velocity dispersion. Section V shows simulation and theoretical results on spectral broadening induced by XPM. Finally, Section VI concludes the paper.

II. SINGLE SPAN

We consider a WDM system composed of one span of single-mode optical fiber, with N copropagating channels having the same polarization.

The nonlinear Schrödinger equation describing the propagation along the z axis of the complex envelope $A_s(z,t)$ of the generic channel s, $s = 1,\ldots,N$, is [3]

$$\frac{\partial A_s(z,t)}{\partial z} + \frac{1}{v_{gs}}\frac{\partial A_s(z,t)}{\partial t} + \frac{\alpha}{2}A_s(z,t) = -j\gamma A_s(z,t)\left[\left|A_s(z,t)\right|^2 + 2\sum_{p\neq s}\left|A_p(z,t)\right|^2\right], \quad (1)$$

where v_{gs} is the group velocity of channel s, α is the attenuation coefficient, γ is the nonlinearity coefficient and the summation is extended to the set of channels $\{p = 1,\ldots,N : p \neq s\}$. The two terms on the right-hand side of (1) give rise to self-phase modulation (SPM) and XPM, respectively. The $-j$ term in (1) appears because of the engineering definition of Fourier transforms [3]. $A +j$ term appears when using the physicist notation [4].

Note that the contributions giving rise to four wave mixing (FWM) have been omitted from the right-hand side of the equation. Thus we suppose we are working with high local GVD, as common in dispersion mapping [5, 6], to effectively suppress FWM.

Note also that on the left-hand side of (1) we have neglected the higher order time derivatives of $A_s(z,t)$, which cause the GVD-induced distortion of the envelope. It is only under this assumption that Eq. (1) can be solved exactly, giving

$$A_s(z,t) = A_s(0, t - z/v_{gs}) e^{-\alpha z/2} e^{j\theta_s(z,t)}, \quad s = 1, \ldots, N, \tag{2}$$

where the signal phase is [1]

$$\theta_s(z,t) = \theta_0 - \gamma \left[L_{\text{eff}}(z) \left| A_s\left(0, t - \frac{z}{v_{gs}}\right) \right|^2 + 2 \sum_{p \neq s} \int_0^z \left| A_p\left(0, t - \frac{z}{v_{gs}} + d_{sp} z'\right) \right|^2 e^{-\alpha z'} \, dz' \right], \tag{3}$$

where θ_0 is the initial phase, and $L_{\text{eff}}(z) = (1 - e^{-\alpha z})/\alpha$ is the effective length of the fiber. The two terms in the squared brackets represent SPM and XPM, respectively.

The coefficient $d_{sp} = v_{gs}^{-1} - v_{gp}^{-1} \simeq D_c \Delta\lambda_{sp}$ [4] is the *walk-off* parameter between channels s and p, where D_c is the dispersion coefficient of the fiber and $\Delta\lambda_{sp}$ is the wavelength distance between the two channels.

This is the case studied in [1] in the frequency domain, using sinusoidally modulated signals. Here we proceed instead in the time domain.

With the variable change $\tau = -z' d_{sp}$, the term related to XPM in (3) can be rewritten as

$$\theta_s^{\text{XPM}}(z,t) = -2\gamma \sum_{p \neq s} \frac{1}{d_{sp}} \int_{-d_{sp} z}^0 \left| A_p\left(0, t - \tau - \frac{z}{v_{gs}}\right) \right|^2 e^{[\alpha(\tau/d_{sp})]} \, d\tau. \tag{4}$$

The above variable change has a physical meaning: integrating in (3) in the space domain is equivalent to integrating in the time domain that part of the $A_p(0,t)$ interfering signal which crosses the reference signal $A_s(0,t)$ during the propagation over the distance z. The relative walk-off between the s and the p channels is $d_{sp}[s/m]$, so that the integral in the time domain has to be extended over a duration $|d_{sp}|z$, as in (4).

In (4) we recognize the convolution integral

$$\theta_s^{\text{XPM}}(z,t) = -2\gamma \sum_{p \neq s} P_p\left(0, t - \frac{z}{v_{gs}}\right) \otimes h_{sp}(t), \tag{5}$$

where $P_p(0,t) = |A_p(0,t)|^2$ is the input power of signal p and $h_{sp}(t)$ is the impulse response of a linear filter $h_{sp}(t)$, which, for both $d_{sp} > 0$ and $d_{sp} < 0$, is given by

$$h_{sp}(t) = \frac{1}{|d_{sp}|} e^{\alpha(t/d_{sp})} \prod \left(\frac{t + d_{sp} z/2}{z|d_{sp}|} \right), \tag{6}$$

where we have used the rectangular function $\prod(\frac{t}{\tau}) \triangleq 1$ for $|t| < \tau/2$, and zero outside.

In Fig. 1 we plot the impulse response $h_{sp}(t)$, for both $d_{sp} > 0$ and $d_{sp} < 0$. Note that when $d_{sp} > 0$, $h_{sp}(t)$ is noncausal. This should not be a surprise, since the p signal travels faster than s, so that during propagation $\theta_s(z,t)$ is affected by the future bits of the p signal.

The peak of $h_{sp}(t)$ near the origin is due to the fact that the p channel is attenuated during propagation, so that the XPM effect is stronger at the beginning of the interaction. When the fiber has no attenuation ($\alpha = 0$), $h_{sp}(t)$ reduces to a rectangle. In the case of no channel walk-off ($d_{sp} = 0$), we have $h_{sp}(t) = L_{\text{eff}}(z)\delta(t)$, so that we obtain the well-known formula $\theta_s^{\text{XPM}}(z,t) = -2\gamma L_{\text{eff}}(z) \sum_{p \neq s} P_p(0, t - z/v_{gs})$.

The Fourier transform of the impulse response (6) is

$$H_{sp}(\omega) = \int_{-\infty}^{\infty} h_{sp}(t) e^{-j\omega t}\, dt = \frac{1 - e^{-(\alpha - j\omega d_{sp})z}}{\alpha - j\omega d_{sp}}. \tag{7}$$

Its squared magnitude and phase are, respectively,

$$|H_{sp}(\omega)|^2 = L_{\text{eff}}^2(z) \frac{1}{1 + (\omega d_{sp}/\alpha)^2} \left[1 + \frac{4e^{-\alpha z} \sin^2(\omega d_{sp} z/2)}{(1 - e^{-\alpha z})} \right] \tag{8}$$

$$\angle H_{sp}(\omega) = \text{arctg}\left(\frac{\sin(\omega d_{sp} z)}{\cos(\omega d_{sp} z) - e^{\alpha z}} \right) + \text{arctg}\left(\frac{\omega d_{sp}}{\alpha} \right). \tag{9}$$

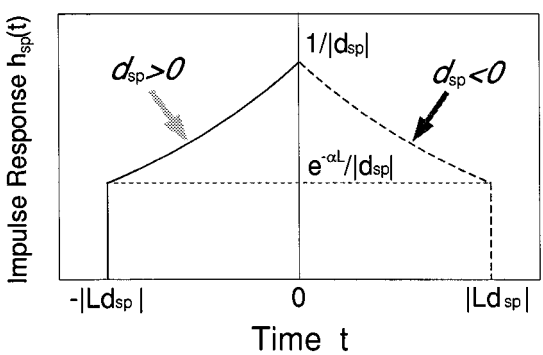

FIG. 1. Impulse response $h_{sp}(t)$ in both cases of positive and negative walk-off parameter.

Equation (8) agrees with the result in [1]. However, (9) gives the correct expression for the phase, while expression (10) of [1] is incorrect.

First, it is has a typo and should read $\phi = -\arg(-\alpha + i\omega d_{12}) + \arg(-(1 - e^{-\alpha L}\cos(\omega d_{12} L)) + ie^{-\alpha L}\sin(\omega d_{12} L))$, which agrees with (9) here.

Second, there is an inconsistency in [1]: the authors start with a version of Eq. (1) derived according to the physicists' notation for Fourier transforms [4], and later they use [1, Eq. (16)] the engineer's notation, as we do here. This is why our expression for ϕ in (9) matches with their ϕ. However, in the physicists' notation, the correct expression is $-\phi$.

From (8) we immediately get the 3-dB bandwidth B_w when the fiber length z is long. In such case the $\sin^2(\ )$ can be neglected and by inspection we see that $B_w = \alpha/|d_{sp}|$. In the limit $d_{sp} \to \infty$ only the DC power component is passed by the filter, so that no XPM is observed.

Figure 2 plots the 3-dB bandwidth B_w, as a function of $\Delta\lambda_{sp}$, for two typical values of dispersion.

Since B_w quickly decreases with $\Delta\lambda_{sp}$, more distant channels are more filtered and give a lower contribution to XPM. This justifies the experimental observation [2] that XPM does not increase linearly with the number of channels N.

III. CASCADE OF AMPLIFIED LINKS

In this section we analyze XPM in the general case of a system composed of $M - 1$ amplifiers, and M links, as in Fig. 3. We suppose that the mth amplifier has gain $G_p^{(m)}$ at the pth wavelength, so that the channel power, after the mth amplifier, is $P_p(L_m, t) = [P_p(L_{m-1}, t)e^{-(\alpha_m l_m)}]G_p^{(m)}$, where α_i and l_i are the atten-

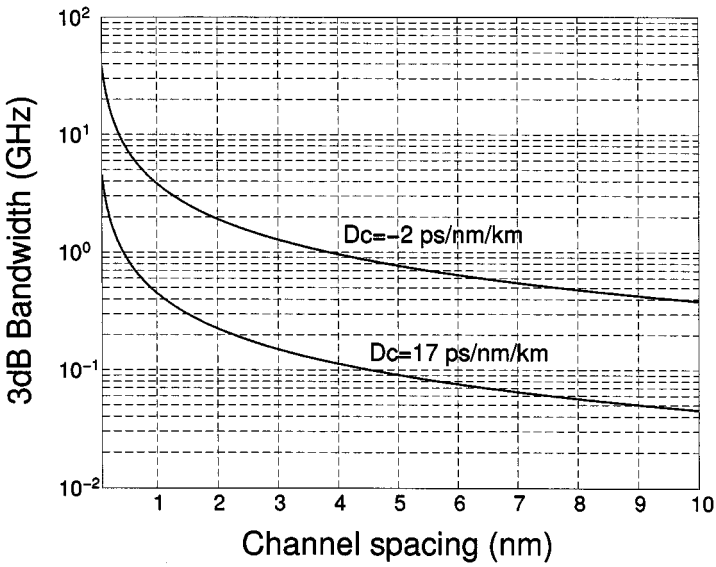

FIG. 2. 3-dB bandwidth $B_w = \alpha/2\pi D_c \Delta\lambda$ versus channel spacing $\Delta\lambda_{sp}$, for $\alpha = 0.21$ dB/km and dispersion $D_c = -2$ and 17 ps/nm/km.

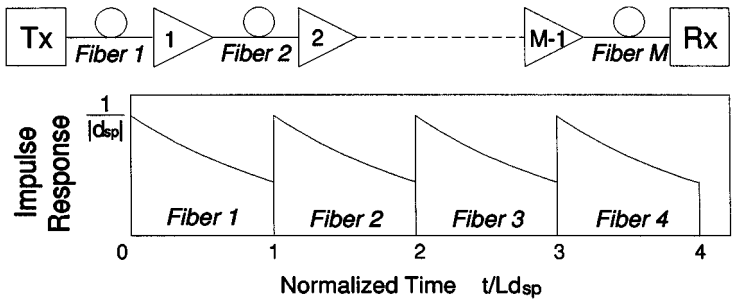

FIG. 3. Top: M concatenated amplified fiber links. Bottom: impulse response in the absence of compensation.

uation coefficient and the length of the ith link, respectively, and $L_m \triangleq \sum_{i=1}^{m} l_i$. The total fiber length is $L = L_M$.

Since, as seen in (3), XPM is given as an integral over the link span, by the linearity of the integral the total XPM at the end of the link can be written as

$$\theta_s^{\mathrm{XPM}}(L,t) = \sum_{i=1}^{M} \theta_s^{\mathrm{XPM}}(l_i,t), \tag{10}$$

whre $\theta_s^{\mathrm{XPM}}(l_i,t)$ is the XPM contribution over the ith link.

In this section it is convenient to write (5) in a time reference moving with velocity v_{gs},

$$\theta_s^{\mathrm{XPM}}(l_i,t) = -2\gamma \sum_{p\neq s} P_p(0,t) \otimes h_{sp}^{(i)}(t), \tag{11}$$

where the superscript (i) indicates the dependence of the impulse response $h_{sp}(t)$, defined in (6), on the length, walk-off, and attenuation parameters l_i, $d_{sp}^{(i)}$, α_i of the ith link.

The XPM at the end of the first link is $\theta_s^{\mathrm{XPM}}(l_1,t) = -2\gamma \sum_{p\neq s} P_p(0,t) \otimes h_{sp}^{(1)}(t)$. The XPM contribution of the second link is

$$\begin{aligned}
\theta_s^{\mathrm{XPM}}(l_2,t) &= -2\gamma \sum_{p\neq s} P_p(l_1,t) \otimes h_{sp}^{(2)}(t) \\
&= -2\gamma \sum_{p\neq s} e^{-\alpha_1 l_1} G_p^{(1)} P_p\left(0, t + l_1 d_{sp}^{(1)}\right) \otimes h_{sp}^{(2)}(t) \\
&= -2\gamma \sum_{p\neq s} P_p(0,t) \otimes \left[C_p^{(2)} h_{sp}^{(2)}\left(t + l_1 d_{sp}^{(1)}\right)\right],
\end{aligned} \tag{12}$$

where $C_p^{(2)} \triangleq e^{-\alpha_1 l_1} G_p^{(1)}$ is the power gain at the beginning of the second link.

From (12) we see that the XPM contribution of the second link can be seen again as a linear filtering of the same input function $P_p(0,t)$. The linear filter is as in (6), but translated in time by $l_1 d_{sp}^{(1)}$ and multiplied by the constant $C_p^{(2)}$.

In general, the XPM contribution of the mth link ($m = 1, \ldots, M$) is

$$\theta_s^{\mathrm{XPM}}(l_m, t) = -2\gamma \sum_{p \neq s} P_p(L_{m-1}, t) \otimes h_{sp}^{(m)}(t)$$

$$= -2\gamma \sum_{p \neq s} P_p(0, t) \otimes \left[C_p^{(m)} h_{sp}^{(m)} \left(t + \sum_{i=1}^{m-1} l_i d_{sp}^{(i)} \right) \right], \qquad (13)$$

where the effective gain at the beginning of the mth link is $C_p^{(m)} \triangleq \prod_{i=1}^{m-1} e^{-\alpha_i l_i} G_p^{(i)}$, and $C_p^{(1)} \triangleq 1$.

By (10), the total XPM at the end of the Mth link is then $\theta_s^{\mathrm{XPM}}(L, t) = -2\gamma \sum_{p \neq s} P_p(0, t) \otimes \hat{h}_{sp}(t)$, where the overall filter impulse response is

$$\hat{h}_{sp}(t) = \left\{ \sum_{j=1}^{M} C_p^{(j)} h_{sp}^{(j)} \left(t + \sum_{i=1}^{j-1} l_i d_{sp}^{(i)} \right) \right\}. \qquad (14)$$

In Fig. 4 we show a block diagram implementing (14). The equivalent filter for channel p is indeed a parallel bank of filters.

For example, consider the simplified case $C_p^{(j)} = 1$, $\forall j$, i.e., the gain $G_p^{(j)}$ of the jth amplifier exactly compensates the loss of the preceding $(j-1)$st fiber link. Suppose furthermore that the links have the same length, attenuation, and walk-off —$l_j = l$, $\forall j$, $\alpha_j = \alpha$, $\forall j$, $d_{sp}^{(j)} = d_{sp}$, $\forall j$— so that we drop the dependence of h_{sp} on j.

In this case, the total overall impulse response simplifies to

$$\hat{h}_{sp}(t) = \left\{ \sum_{k=0}^{M-1} h_{sp}(t + kld_{sp}) \right\} \qquad (15)$$

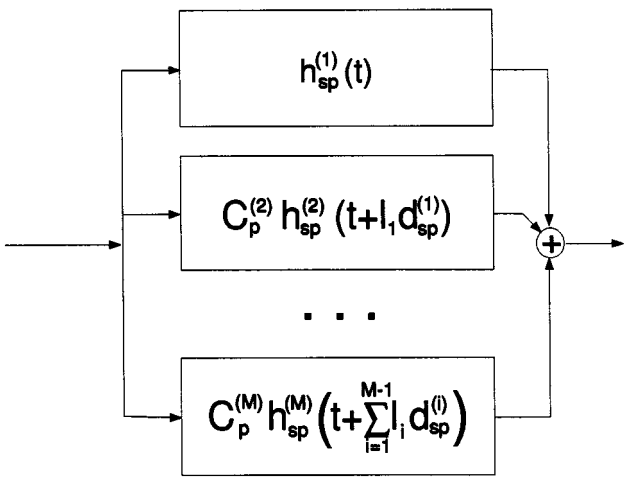

FIG. 4. Graphical interpretation of Eq. (14).

and taking Fourier transforms

$$\hat{H}_{sp}(\omega) = H_{sp}(\omega)\left\{\sum_{k=0}^{M-1} e^{j\omega k l d_{sp}}\right\}$$
$$= H_{sp}(\omega)\, e^{j\omega l d_{sp}(M-1)/2}\left(\frac{\sin(M\omega l d_{sp}/2)}{\sin(\omega l d_{sp}/2)}\right) \tag{16}$$

the same result obtained in [1].

Equation (14) is extremely general. It can be used for any type of multistage system, with any amplifier gain profile, with any kind of compensating scheme.

In Fig. 3 we show an example of $\hat{h}_{sp}(t)$ in the case of a noncompensated system, composed of M identical links, when the amplifiers exactly compensate the fiber loss. The overall impulse response is just the sum of the M shifted copies of the basic filter (6).

In Fig. 5 we show the case of a compensated system with imperfect compensation, composed of $M = 4$ identical spans of transmission fiber, each followed by a span of compensating fiber of opposite dispersion and an amplifier to exactly recover the span loss. The figure shows the individual contributions of each fiber segment to the overall impulse response. As opposed to Fig. 3, note that here the (identical) contributions of the transmission fibers are partially overlapping, because of the backward relative walk-off achieved by the compensating fibers, which brings the s and p channels back aligned, although not exactly. In this example the responses of the compensating fibers are noncausal. The compensating fibers, when placed at the end of each transmission span, give typically only a small contribution to the overall filter response $\hat{h}_{sp}(t)$ and thus can be safely neglected. In the case of a perfectly compensated M-span system, neglecting the contribution of the compensating fibers at each link, we obtain $\hat{h}_{sp}(t) \simeq M h_{sp}^{(1)}(t)$, so that the XPM effect is M times larger than that of a single link.

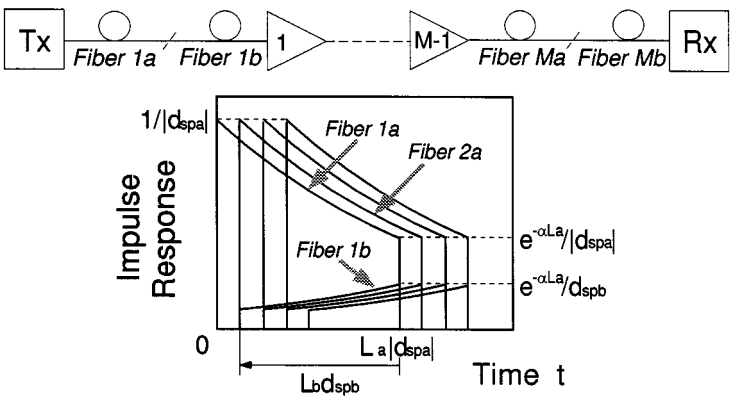

FIG. 5. Individual fiber contributions to the overall impulse response of an imperfectly compensated system. The overall response is the sum of those shown.

IV. SIMULATIONS

We wanted to check how sensitive the results of the present model are when the underlying assumption of undistorted field envelopes used to derive the model is violated.

In Figs. 6 and 7 we show the results of computer simulations, performed by the split-step Fourier method [4].

Simulations are carried out for a multi-span WDM system, with 10 spans, 2 channels, and 3 mW peak power per channel, of the compensated type depicted in Fig. 5. One of the channels (pump) is on–off keying (OOK) modulated with raised cosine pulses with roll-off 0.5, at a bit rate $R = 10$ Gb/s, while the other (probe) is unmodulated.

Figure 6 refers to a system in which at each span the transmission fiber is a nonzero dispersion fiber (NZDF), with dispersion $D = -2$ ps/nm/km and length $l = 85$ km, and a standard single-mode fiber (SMF) with $D = 17$ ps/nm/km and $l = 10$ km is used for span compensation. Other parameters common to the two fibers are dispersion slope $D' = 0.07$ ps/km/nm^2, nonlinear coefficient $\gamma = 2.34$ W^{-1} km^{-1}, attenuation $\alpha = 0.21$ dB/km.

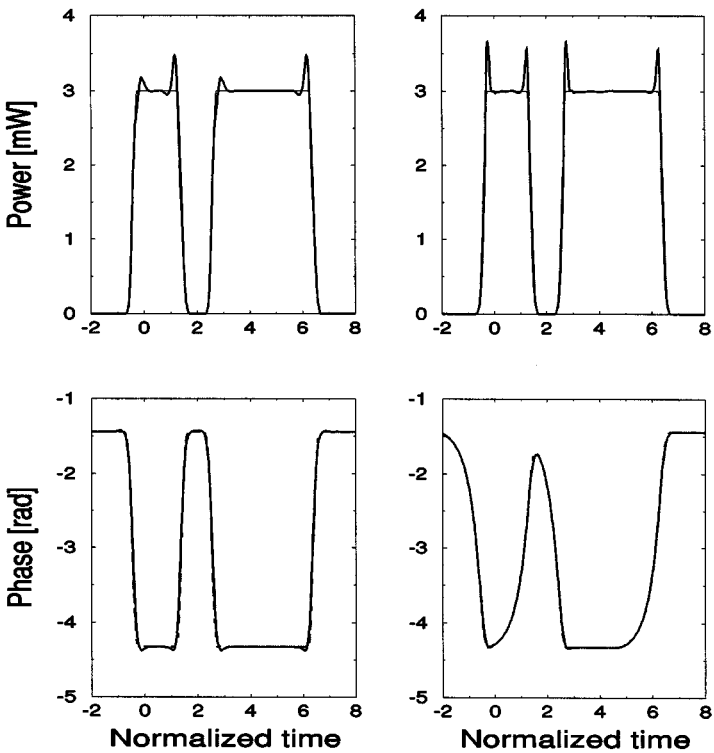

FIG. 6. Simulations of a NZDF compensated system, $R = 10$ Gb/s, $M = 10$ spans. Left column: $\Delta\lambda = 0.1$ nm. Right column: $\Delta\lambda = 1$ nm. Top row: Pump power (mW). Bottom row: phase of probe signal (rad). Time is normalized to the bit time $1/R$.

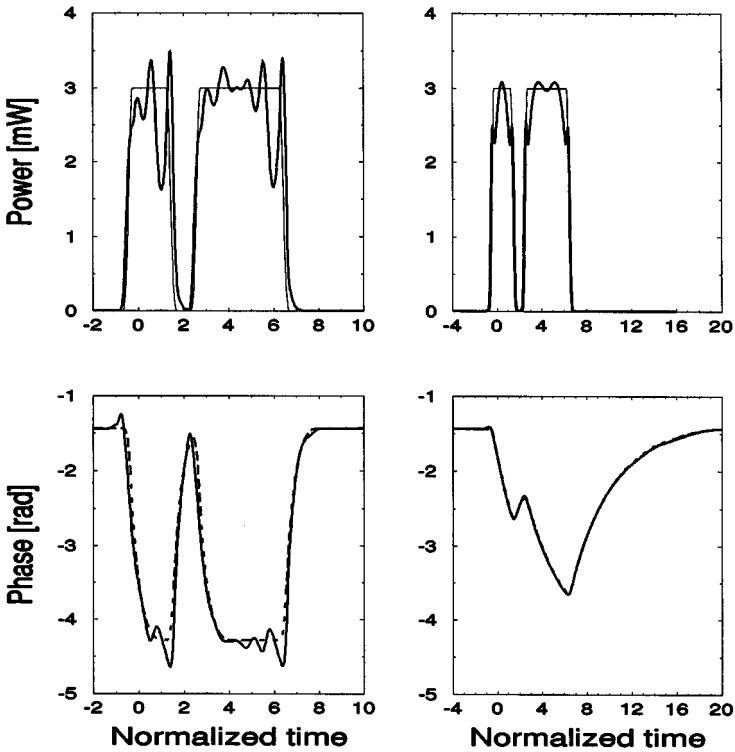

FIG. 7. Simulations of a SMF compensated system, $R = 10$ Gb/s, $M = 10$ spans. Left column: $\Delta\lambda = 0.1$ nm. Right column: $\Delta\lambda = 1$ nm. Top row: Pump power (mW). Bottom row: phase of probe signal (rad). Time is normalized to the bit time $1/R$.

Figure 7 refers to a system in which the transmission fiber is SMF, with $l = 76$ km, $D = 17$ ps/nm/km, $D' = 0.07$ ps/km/nm^2, $\gamma = 2.35$ W^{-1} km^{-1}, $\alpha = 0.21$ dB/km, and a dispersion compensating fiber (DCF) with $l = 13.6$ km, $D = -95$ ps/nm/km, $D' = 0.07$ ps/km/nm^2, $\gamma = 5$ W^{-1} km^{-1}, $\alpha = 0.6$ dB/km, is used for compensation.

In both figures, the wavelength of exact compensation is halfway between channels. The figures show both the power of the pump (top) and the phase of the probe (bottom) at the end of the system. The pattern ''1101111'' is visible in the pump intensity. In the phase plots, the theoretical predictions of the model, obtained by (14), are shown in bold dashed lines. The right column refers to a system with channel spacing $\Delta\lambda = 1$ nm, while the left column refers to a system with $\Delta\lambda = 0.1$ nm. In both cases, the pump intensity distortion induced by GVD is quite evident. For the 1 nm spacing case, the match between theory and simulations is excellent. This is due to the low-pass filtering effect connected to GVD-induced channel walk-off.

For example, in Fig. 6 for 1-nm spacing the XPM filter bandwidth, as seen from Fig. 2, is $B_w = 3.85$ GHz, which is enough to mildly smooth out in the probe phase the original 10 Gb/s NRZ pump modulation and to substantially filter away from

the modulating intensity the GVD-induced high-speed phase-to-intensity (PM/IM) fluctuations.

In fact, the peak frequencies of the PM/IM spectrum are [7] $f_p = \sqrt{n}\,\frac{1}{\lambda}\sqrt{\frac{c}{2LD}}$, where c is the speed of light and $n = 1, 2, \ldots$. In our case, the lowest peak is at $f_p = 19$ GHz.

The 0.1-nm spacing case was selected to show how small the walk-off should be for the low-pass filtering not to be effective, although our simulations take into account only SPM and XPM, and not FWM, which in this case may be the dominant impairment.

For example, in Fig. 6 for 0.1-nm spacing the XPM filter bandwidth is 10 times larger than before, $B_w = 38.5$ GHz, so that the NRZ probe modulation is passed with little distortion, while the high-speed PM/IM fluctuations are a little less suppressed than in the previous case.

In Fig. 7 we first note that the shape of the phase is reversed, since in the SMF-compensated case the sign of dispersion and thus of walk-off is reversed. The conclusions we reach about the effectiveness of filtering are similar, although the discrepancy between model and simulation is larger. This seems at first sight surprising, since the walk-off in the transmission fiber is larger with a dispersion of 17 ps/nm/km.

However, although the filtering is better, the intensity fluctuations due to PM/IM conversion at the time points perturbated by XPM and SPM have substantial frequency components below 10 Gb/s. In this case in fact we get the lowest PM/IM peak at $f_p = 7$ GHz. Such components are not filtered by walk-off and account for the larger error in the model.

V. APPLICATIONS

The explicit expression (14) of the impulse response $\hat{h}_{sp}(t)$ is fundamental to analytically evaluating the transmission impairments induced by XPM in multi-span systems. Here, we use (14) to give an evaluation of the spectral broadening due to XPM in multi-span compensated systems.

Suppose $A_p(0,t)(p = 1, \ldots, N)$ is an OOK/NRZ modulated signal, of the form $A_p(0,t) = \sqrt{P_s(0)}\,B_s(0,t)$, where $P_s(0)$ is the signal mark power at the transmitter, and $B_s(0,t) = \sum_{k=-\infty}^{\infty} a_s(k)p(t - kT - \delta_s)$ is the OOK modulating signal at the fiber input, where $a_s(k)$ is a sequence of independent random variables taking value 1 for mark and 0 for space with equal probability, $p(t)$ is the supporting pulse, T is the bit time, and δ_s is a random delay uniformly distributed between $[-T/2, T/2]$. It is shown in [8] that the autocorrelation of the output stationary process $A_s(z,t)$ in Eq. (2) is

$$R_{A_s}(\tau) = P_s(z) \cdot R_s(\tau) \cdot R_{\mathrm{XPM}}(\tau), \tag{17}$$

where $P_s(z)$ is the signal mark power at the receiver,

$$R_s(\tau) = \frac{1}{4}\left[1 + \Lambda\left(\frac{\tau}{T}\right)\right] \tag{18}$$

is the contribution of the OOK/NRZ modulation, $\Lambda(\frac{\tau}{T})$ being the triangular function [9], and $R_{\mathrm{XPM}}(\tau)$ is the XPM contribution. In the case of a large number N of input channels, the distribution of the random phase process $\theta_s^{\mathrm{XPM}}(z,t)$ becomes approximately Gaussian, so that we can write

$$R_{\mathrm{XPM}}(\tau) = e^{-\sigma^2(\tau)/2}, \tag{19}$$

where $\sigma^2(\tau)$ is the variance of the process $-2\gamma \sum_{p \neq s} [B_p(0,t) - B_p(0,t-\tau)]P_p(0) \otimes \hat{h}_{sp}(t)$. This variance can be analytically calculated and has a rather complicated but closed form [10]. This computation requires explicit knowledge of the impulse response (14).

The power spectrum, i.e., the Fourier transform of (17), has been compared with computer simulations. Figure 8 shows the results for an 8-channel NZDF-compensated system with $M = 5$ spans. The system parameters are those of section IV. The only differences are the bit rate $R = 2.5$ Gb/s, and the channel spacing $\Delta\lambda = 0.4$ nm. In the figure both the simulated and the analytically calculated power spectrum of the 4th channel are plotted, together with the input OOK spectrum. We can note a very good match between the simulation results and the analytical ones.

VI. CONCLUSIONS

In future high-speed IM/DD WDM transmission systems with appropriate dispersion management, after FWM has been properly suppressed, the main cause of eye closure and thus of system degradation will be the two remaining nonlinear Kerr effects, SPM and XPM.

It is thus important to be able to accurately predict XPM, in order to estimate its local perturbation of the compensation of dispersion, which gives rise to the residual intensity distortion and thus eye closure.

This paper has given a time-domain derivation of the very important model for XPM presented in [1]. A simple and very general expression for the impulse response of the XPM filters in the model has been presented.

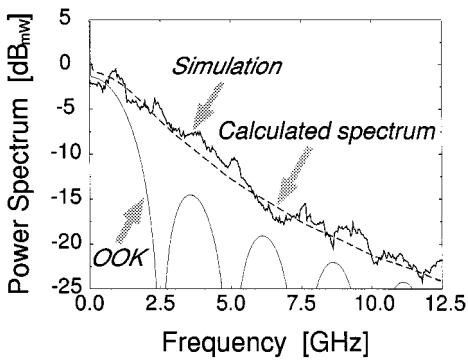

FIG. 8. Simulations of a NZDF compensated system, $N = 8$, $R = 2.5$ Gb/s, $M = 5$ spans, $\Delta\lambda = 0.4$ nm.

While such filters are obtained in the assumption of undistorted field intensities on all channels, simulation results show that the model still accurately predicts the XPM even in the presence of strong intensity distortion.

This unobvious result implies that the modulation induced on the optical field phase by XPM is nearly independent of the distortion induced on the intensity of the optical field by group velocity dispersion.

This is true in the cases shown here, bit rate 10 Gb/s and wavelength spacing larger than 0.1 nm, $M = 10$ spans of about 90 km each, for both an NZDF and an SMF compensated system.

The model clearly holds for higher bit rates, as the XPM filter bandwidth is independent of the bit rate. For the same systems at a lower rate, we have to increase the number of spans to much larger M to observe a comparable distortion on the intensity. However the phase error between theory and simulation should remain small as in the 10 Gb/s case, since the rapid fluctuations due to PM/IM conversion get filtered as effectively as in the 10 Gb/s case.

Finally, as an application of the theory, we have shown that the spectral broadening induced by XPM can be accurately predicted.

ACKNOWLEDGMENT

This work was supported by the European Community under INCO-DC Project 950959 ''DAWRON.''

REFERENCES

[1] T. Chiang, N. Kagi, M. E. Marhic, and L. Kazovsky, ''Cross-phase modulation in fiber links with multiple optical amplifiers and dispersion compensators,'' *IEEE J. Lightwave Technol*., vol. 14, 249 (1996).

[2] D. Marcuse, A. R. Chraplyvy, and R. W. Tkach, ''Dependence of cross-phase modulation on channel number in fiber WDM systems,'' *IEEE J. Lightwave Technol*., vol. 12, 885 (1994).

[3] D. Marcuse, *Theory of Dielectric Optical Waveguides*, 2nd ed., chap. 9, Academic Press, San Diego, 1991.

[4] G. W. Agrawal, *Nonlinear Fiber Optics*, 2nd ed., chap. 7, Academic Press, San Diego, 1995.

[5] C. Kurtzke, ''Suppression of fiber nonlinearities by appropriate dispersion management,'' *IEEE Photon. Technol. Lett*., vol. 5, 1250 (1993).

[6] A. R. Chraplyvy, A. H. Gnauck, R. W. Tkach, R. M. Derosier, C. R. Giles, B. M. Nyman, G. A. Ferguson, J. W. Sulhoff, and J. L. Zyskind, ''One-third terabit/s transmission through 150 km of dispersion-managed fiber,'' *IEEE Photon. Technol. Lett*., vol. 7, 89 (1995).

[7] J. Wang and K. Petermann, ''Small signal analysis for dispersive optical fiber communication systems,'' *IEEE J. Lightwave Technol*., vol. 10, 96 (1992).

[8] G. Bellotti, C. Francia, and A. Bononi, ''Spectral broadening due to cross-phase modulation (XPM) in OOK WDM transmission systems,'' in *Proceedings, LEOS'97 10th Annual Meeting*, San Francisco, CA, pp. 226–227, paper WAA3, 1997.

[9] B. Carlson, *Communication Systems*, 3rd ed., p. 668, McGraw–Hill, New York, 1986.

[10] G. Bellotti, *Laurea Thesis*, Dip. Ing. dell'Informazione, Università di Parma, 1997.